physica status solidi

pss

www.pss-journals.com

reprint

WILEY-VCH

Wiley Online Library
Early View publication on www.wileyonlinelibrary.com
(issue and page numbers not yet assigned;
citable using Digital Object Identifier – **DOI**)

Phys. Status Solidi A, 1–8 (2014) / **DOI** 10.1002/pssa.201300218

physica status solidi a
www.pss-a.com
applications and materials science

A thermoelectric generator based on an n-type clathrate and a p-type skutterudite unicouple

E. Alleno*[,1], N. Lamquembe[1], R. Cardoso-Gil[2], M. Ikeda[3], F. Widder[3], O. Rouleau[1], C. Godart[1], Yu. Grin[2], and S. Paschen[3]

[1] Institut de Chimie et Matériaux Paris-Est, UMR 7182 CNRS – UPEC, 2–8, rue Henri Dunant, 94320 Thiais, France
[2] Max Planck Institute – Chemical Physics of Solids, Nöthnitzer Straße 40, 01187 Dresden, Germany
[3] Institute of Solid State Physics, Vienna University of Technology, WiednerHauptstraße 8–10, 1040 Vienna, Austria

Received 17 June 2013, revised 26 November 2013, accepted 4 March 2014
Published online 8 May 2014

Keywords clathrate, generator, skutterudite, thermoelectricity

* Corresponding author: e-mail eric.alleno@icmpe.cnrs.fr, Phone: +33 1 4978 1237, Fax : +33 1 4978 1203

The type I clathrates $A_8Ga_{16}X_{30}$ (A = Sr, Ba, Eu; X = Si, Ge, Sn) and filled skutterudites $A_y(Fe_{1-x}M_x)_4Sb_{12}$ (A = rare-earth, M = Co, Ni,) are intermetallic compounds with good thermoelectric performance in the temperature range 400–800 K. Here we report on the first mixed clathrate–skutterudite unicouple thermoelectric generator and address important technical issues such as upscaling, contacting, and electrode material selection. At 600 K, the materials $Eu_8Ga_{16}Ge_{30}$, $Ba_8Ga_{16}Ge_{30}$, and $Mm_{0.7}Fe_{3.5}Ni_{0.5}Sb_{12}$ synthesized for this purpose have figures of merit $ZT = 0.32$, 0.15, and 0.46, respectively. The clathrate and skutterudite legs were brazed to a hot side nickel electrode. An average contact resistivity of 16 $\mu\Omega\,cm^2$ was obtained with Pb–Ag (hot side) and In–Sn (cold side) brazings combined with and intermediate Ni layer. For a temperature difference $\Delta T = 250$ K (hot side temperature = 573 K), this generator produced an open circuit voltage $U_{open} = 54$ mV and an electrical specific power $P = 178\,mW\,cm^{-2}$ as our best result with the couple $Mm_{0.7}Fe_{3.5}Ni_{0.5}Sb_{12}$ and $Eu_8Ga_{16}Ge_{30}$.

1 Introduction Thermoelectric (TE) solid state devices are currently considered by the automobile industry [1–3] to recover and partially convert into electricity the heat wasted by vehicles with gas engines (radiator, exhaust pipe). This could improve the overall energy efficiency of these vehicles and lead to fuel savings. TE generators (TEGs) bear several advantages over alternative solutions to recover waste heat such as a Sterling engine, for instance [4]. They are simple, compact, silent, and highly reliable (no moving parts). The efficiency of such devices not only depends on the temperature difference between the cold and hot side but also on the dimensionless TE figure of merit (ZT) of the p- and n-type constituting materials. Until the late 1980s, the best materials had maximum ZT values ranging from 0.6 at 1000 K for Si–Ge and 0.7 at 700 K for PbTe derivatives to 1.0 at 300 K for Bi_2Te_3 derivatives [5]. With a typical maximum hot side temperature of 750 K for the exhaust pipe, a device based on a material with a maximum $ZT = 0.7$ would show a practical efficiency of ~5%. This efficiency is too low to plan mass production of thermoelectricity. However, the discovery of new materials with maximum ZT larger than 1 in the late 1990s such as the skutterudites [6–8] and the clathrates [9, 10] changed this situation. TE devices based on these materials should be able to reach 8–10% of efficiency for a hot side temperature of 800 K and should thus play an important role in this search of reduced fossil fuel consumption.

TE type I clathrates are compounds with the generic formula $A_8M_xX_{46-x}$ where X = Si, Ge, Sn, and M is a metal from column VIII, IB, IIB, or IIIA which partially substitutes the element X. A is an alkaline-earth or a divalent rare-earth element. The M/X atoms form large cages (20 or 24 atoms) which are filled by the A atoms. The A atoms display large localized vibrations which on one hand resonantly scatter the acoustic phonons and on the other hand reduce the mean phonon velocity [11, 12], leading to strongly reduced lattice thermal conductivities (λ_L). Polycrystalline semiconducting $Ba_8Ga_{16}Ge_{30}$ displays a maximum ZT value of 0.7 at 700 K and an average value $ZT_{av} = 0.3$ over the temperature interval 300–700 K [13, 14] while single crystalline

$Ba_8Ga_{16}Ge_{30}$ displays ZT values ranging from 0.8 at 1050 K [14] to a maximum $ZT = 1.35$ at 900 K ($ZT_{av} = 0.63$ over 400–800K) [10]. More recently, $ZT = 1.2$ at 1000 K, $ZT = 1.1$ at 950 K, $ZT = 0.9$ at 680 K and $ZT = 0.9$ at 800 K were respectively reported in $Ba_8Ni_xZn_yGa_zGe_{30-x-y-z}$ [15], in $Yb_{0.5}Ba_{7.5}Ga_{16}Ge_{30}$ [16], in $Ba_8Au_xGe_{46-x}$ [17], and in $Ba_8Zn_{7.22}Ni_{0.22}Ge_{37.12}Sn_{1.44}$ [18]. The TE properties of semiconducting n-type $Eu_8Ga_{16}Ge_{30}$ are less well established. The high temperature thermal conductivity data (up to 750 K) published in Ref. [19] is an extrapolation from low temperature measurements (200 K). $Eu_8Ga_{16}Ge_{30}$ thus displays an estimated maximum ZT value of 1.1 at 750 K and an estimated average $ZT_{av} = 0.85$ over the temperature range 300–750 K [19]. No p-type $Eu_8Ga_{16}Ge_{30}$ has ever been reported while the maximum ZT values of p-type $Ba_8Ga_{16}Ge_{30}$ are rather scattered in literature: from 0.4 in Ref. [20], 0.5 in Ref. [21] at 800 K to 1.0 at 900 K in Ref. [22]. This is why we chose a skutterudite as a p-leg.

TE skutterudites are antimonides with the generic formula $A_y(MM')_4Sb_{12}$ $(0 < y < 1.0)$, where A is an electropositive element (alkaline, alkaline-earth, or rare-earth elements) or a mixture of electropositive elements, and M and M′ are transition metals of the Fe, Co, or Ni columns. Structurally, the A atom fills a large Sb cage and contributes, just as in the clathrates, to low-energy vibration modes that reduce the lattice thermal conductivity: for instance $\lambda_L \sim 1.2\,W\,m^{-1}\,K^{-1}$ was observed in $Ce_yFe_{4-x}Co_xSb_{12}$ at 300 K [23, 24]. Skutterudites display good TE performances both as p-type and n-type materials between 400 and 800 K. The best values for non-nanostructured material are $ZT = 1.7$ in n-type $Ba_{0.08}La_{0.05}Yb_{0.04}Co_4Sb_{12}$ at 850 K [25] and $ZT = 1.2$ in p-type $Pr_{0.033}Nd_{0.62}Fe_3CoSb_{12}$ at 800 K [26]. p-type $Mm_yFe_{4-x}(Co/Ni)_xSb_{12}$ skutterudites were first reported in Ref. [27] and their TE properties at high temperature are reported in Ref. [28]. These skutterudites bear the advantage of being composed of a cheaper mixture of rare earths, e.g. La, Ce, Pr, and Nd = "Mischmetall (Mm)". p-type $Mm_{0.8}Fe_3CoSb_{12}$ displays a maximum $ZT = 1.1$ at 800 K [28] and an average figure of merit $ZT_{av} = 0.7$.

To push these materials towards applications, we designed and built a unicouple TE generator using either $Eu_8Ga_{16}Ge_{30}$ or $Ba_8Ga_{16}Ge_{30}$ as the n-type leg and $Mm_{0.7}Fe_3CoSb_{12}$ or $Mm_{0.7}Fe_{3.5}Ni_{0.5}Sb_{12}$ as the p-type leg. A unicouple generator (Fig. 1) is the simplest and most flexible system to test samples and contacting methods: samples can be easily installed, removed, and replaced, the temperature and the branch resistance can be measured precisely, and modeling is straightforward. Despite the larger specific power generated by an "all skutterudite" generator [29], considering a clathrate as the n-leg brings the partial advantage of using elements (Ba, Ga, Ge) with fewer economical or political tensions for their market than those of skutterudites (rare earth, Sb) [30].

$Ba_8Ga_{16}Ge_{30}$ melts congruently at 1247 K (974 °C) while $Eu_8Ga_{16}Ge_{30}$ (type-I structure) melts at 969 K (696 °C) [31]. From thermal analysis, $Yb_{0.4}Ce_{0.3}Fe_3CoSb_{12}$ and $Mm_{0.7}Fe_{3.5}Ni_{0.5}Sb_{12}$ decompose peritectically at 1010 K (740 °C) and at 1020 K (750 °C), respectively. Hence these materials are thermally stable up to at least 1000 K in inert atmosphere. In air, oxidation starts at 630 K (360 °C) in $Eu_8Ga_{16}Ge_{30}$ [31]; the skutterudite $CeFe_4Sb_{12}$ oxidizes and decomposes at 573 K (300 °C) in air [32]. We thus chose to limit the maximum hot side temperature to 573 K (300 °C).

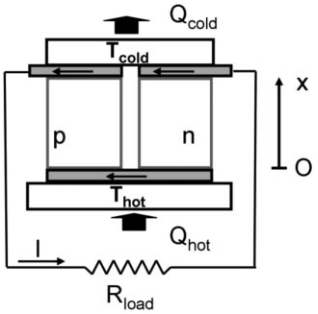

Figure 1 Schematic representation of a unicouple.

2 Unicouple modeling The main parameters characterizing the unicouple are the output power (P_e) and the open circuit voltage (U_{open}). To check whether the unicouple is operated under optimum conditions it is essential to compare these measurements with values expected from the temperature-dependent transport coefficients (electrical resistivity $\rho(T)$, Seebeck coefficient $\alpha(T)$, thermal conductivity $\lambda(T)$). To calculate these parameters, we therefore used a model which is a simplification of a 1D model initially developed by El-Genk and Saber [33] for segmented unicouples. To determine the temperature field $T_n(x)$ and $T_p(x)$ in each leg, this model assumes that the temperature-dependent transport coefficients of Domenicali's equation [34] can be replaced by their spatial average over the length l of the thermoelements [33]:

$$\bar{\lambda}_i = \frac{1}{l}\int_0^l \lambda_i\,(T(x))\,\mathrm{d}x;\ \bar{\rho}_i = \frac{1}{l}\int_0^l \rho_i\,(T(x))\,\mathrm{d}x;$$

$$q_{\tau_i} = -\frac{j_i}{l}\int_0^l T_i\,(x)\,\frac{\mathrm{d}T_i}{\mathrm{d}x}\,\frac{\mathrm{d}\alpha_i}{\mathrm{d}T_i}\,\mathrm{d}x,$$

with $i = p$, n, and ρ the resistivity (the parameters are defined in Table 1). This leads in each leg to these two simplified differential equations:

$$\bar{\lambda}_i\,\frac{\mathrm{d}^2T}{\mathrm{d}x^2} + \bar{\rho}_i j_i^2 + q_{\tau_i} = 0. \qquad (1)$$

Equation (1) must be solved iteratively since each current density $j_i = I/A_i$ depends on each $T_i(x)$. Provided that the following four boundary conditions, $T_i(0) = T_{hot}$ and $T_i(l) = T_{cold}$ are fulfilled, the following analytical expression

Table 1 Calculations of the output power and efficiency of a unicouple made of n-type $Eu_8Ga_{16}Ge_{30}$ and p-type $Yb_{0.4}Ce_{0.4}Fe_3CoSb_{12}$ and based on transport data taken from Refs. [19] and [35] respectively.

input parameters		
T_C [a]	323	323
T_H [b]	773	573
l [c]	6	6
A_p [d]	1	1
ρ_c [e]	0	0
calculated parameters		
A_n/A_p [f]	2.22	2.04
U_{open} [g]	156.6	76.9
R_{thm} [h]	1.18	1.08
R_{opt} [i]	1.56	1.33
I [j]	57.3	31.9
Q_{hot} [k]	50.3	24.3
P_e [l]	5.11	1.36
P_{es} [m]	1.590	0.447
η [n]	10.2	5.6
η_n [o]	17.5	12.8
ZT_{av} [p]	0.70	0.52

[a]Cold temperature (K).
[b]Hot temperature (K).
[c]Thermoelement length (mm).
[d]Area of the p-leg (cm^2).
[e]Specific contact resistance ($m\Omega\,cm^2$).
[f]Optimum n-leg over p-leg area ratio.
[g]Open-circuit voltage (mV).
[h]Thermoelement resistance ($m\Omega$).
[i]Optimum load resistance.
[j]Current (A).
[k]Input heat at the hot side (W).
[l]Output power (W).
[m]Specific electric power ($W\,cm^{-2}$).
[n]Efficiency (%).
[o]Efficiency normalized by Carnot efficiency (%).
[p]Average ZT over [T_H, T_C].

is derived:

$$T_i(x) = T_{hot} - (T_{hot} - T_{cold})\frac{x}{l} + \frac{q_{\tau_i} + \overline{\rho_i} j_i^2}{2\overline{\lambda_i}} l^2 \left(\frac{x}{l} - \left(\frac{x}{l}\right)^2\right). \quad (2)$$

Since $T_i(x)$ is now known, U_{open} is obtained from the relation: $U_{open} = (\bar{\alpha}_p - \bar{\alpha}_n)(T_{hot} - T_{cold})$, where $\bar{\alpha}_i = \frac{1}{l}\int_0^l \alpha_i(T_i(x))\,dx$ is the average Seebeck coefficient in each leg deduced from the experimental values. Similarly, $P_e = R_{load} \times I^2$ with the current I obtained from $I = U_{open}/(R_{load} + R_{thm} + R_{contact})$ and R_{thm} given by $R_{thm} = (\bar{\rho}_p l/A_p) + (\bar{\rho}_n l/A_n)$. Finally, the input thermal power at the hot side is given by

$$Q_{hot} = \frac{(T_{hot} - T_{cold})}{l}(\bar{\lambda}_p A_p + \bar{\lambda}_n A_n) - \frac{(R_{thm} + R_{contact})I^2}{2} - \frac{(\beta_p + \beta_n)T_{hot}I}{2} + (\alpha_p(T_{hot}) - \alpha_n(T_{hot})) \times T_{hot} \times I,$$

where $\beta_p = (T_{cold}/T_{hot})(\bar{\alpha}_p - \alpha_p(T_{cold})) + (\alpha_p(T_{hot}) - \bar{\alpha}_p)$ and $\beta_n = (T_{cold}/T_{hot})(\alpha_n(T_{cold}) - \bar{\alpha}_n) + (\bar{\alpha}_n - \alpha_n(T_{hot}))$.

The efficiency is finally deduced from $\eta = P_e/Q_{hot}$.

The results of such calculations are reported in Table 1. The ratio of the area of each branch of the unicouple and the load resistance were calculated to maximize the efficiency (maximum efficiency ratio) and we took zero contact resistance and $l = 6$ mm as an arbitrary length for the two legs. Table 1 shows that with $T_H = 773$ K (500 °C) close to the high temperature of an exhaust pipe, a couple of these materials could produce a specific power of 1.59 $W\,cm^{-2}$ and reach a 10% efficiency. When $T_H = 573$ K, the efficiency is reduced because of the smaller Carnot efficiency and because the average figure of merit of both legs is also reduced in this temperature range. This leads nonetheless to a ~5% absolute efficiency and a specific electric power of nearly 450 $mW\,cm^{-2}$. This model can also be used to calculate the dependence of the output power and efficiency on the contact resistance. Here, the specific contact resistance (ρ_c) is the average contact resistance multiplied by the average leg area and it is related to the total contact resistance (R_c) used in the model by the relation: $\rho_c = R_c((A_n + A_p)/8)$. Taking $T_H = 573$K and $T_C = 323$K and the same transport parameters as in Table 1, the calculated output power normalized by the maximum value (P_{enor}) and normalized efficiency (η_{nor}) are shown in Fig. 2 as a function of ρ_c. As expected, both quantities strongly decrease when the specific contact resistance increases: this reflects Joule losses in the contact. They are not equal because the maximum efficiency regime slightly differs from the maximum power regime. When $\rho_c = 20\,\mu\Omega\,cm^2$, the normalized efficiency and output power are still respectively equal to 96% and 95% but both respectively decrease to 83% and 80% when $\rho_c = 100\,\mu\Omega\,cm^2$.

3 Thermoelement synthesis and shaping The clathrates were synthesized by melting the elements in a vitreous carbon crucible by inductive heating. The tested nominal compositions spanned the intervals $A_8Ga_{16+x}Ge_{30-x}$ ($-0.5 \le x \le 0.5$) with A = Eu, Ba. The $Eu_8Ga_{16}Ge_{30}$ buttons were subsequently pre-heated at

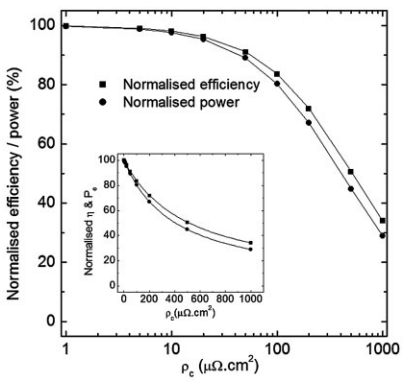

Figure 2 Normalized efficiency (η_{nor}) and normalized electrical power (P_{enor}) as a function of the specific contact resistance.

715 °C for 3 h and annealed at 630 °C for 21 days while the $Ba_8Ga_{16}Ge_{30}$ buttons were annealed for 6 days at 850 °C. The skutterudites $Yb_{0.4}Ce_{0.4}Fe_3CoSb_{12}$ and $Mm_{0.8}Fe_{3.5}Ni_{0.5}Sb_{12}$ were obtained by arc melting the elements in stoichiometric amounts (Ar atmosphere). Only for the rare-earth elements, a 5% excess was added to compensate for evaporation and oxidation. The buttons were subsequently homogenized by re-melting at 1050 °C and annealed for 6 days at 640 °C. More details about the synthesis of both the clathrates and skutterudites can be found in Refs. [13, 36, 37].

Type I $Eu_8Ga_{16}Ge_{30}$ has a limited stability temperature interval and can therefore not be sintered. Thus, it was cut into discs right after annealing. $Ba_8Ga_{16}Ge_{30}$ was crushed into a fine powder, sieved at 50 μm and spark plasma sintered (SPS) in a graphite die at 700 °C during 12 min under a pressure of 80 MPa. Similarly, $Mm_{0.7}Fe_{3.5}Ni_{0.5}Sb_{12}$ was crushed and sieved into a 36 μm powder and spark plasma sintered at 500 °C during 60 min under 50 MPa. Archimedian relative densities of respectively 94% and 97% were measured for the $Ba_8Ga_{16}Ge_{30}$ and skutterudites samples.

4 Thermoelectric properties $\rho(T)$ and $\alpha(T)$ were measured with a ZEM-3 (ULVAC-Riko, Japan), $\lambda(T)$ was calculated via $\lambda = d \times C_p \times a$ from the thermal diffusivity a, measured by the laser flash method with a Flashline-3000 system (ANTER, USA), the bulk density d and the specific heat C_p calculated from the Dulong–Petit law. The lattice thermal conductivity was obtained from Wiedeman–Franz law taking $2.2 \times 10^{-8}\,W\Omega\,K^{-2}$ as Lorentz number.

Figure 3 compares the high-temperature TE performance of two of the samples synthesized in this work ($Eu_8Ga_{16}Ge_{30}$-rc8105 and $Ba_8Ga_{16}Ge_{30}$-rc41) with published results: the five $Eu_8Ga_{16-x}Ge_{30+x}$ samples labeled β_1–β_5 taken from Ref. [38] and the polycrystalline $Ba_8Ga_{16}Ge_{30}$ sample studied in Ref. [14] and labeled "Toberer." The power factor of $Eu_8Ga_{16}Ge_{30}$-rc8105 is substantially smaller than the power factors of the $Eu_8Ga_{16-x}Ge_{30+x}$ samples β_1–β_3 but close to the power factors of β_4 and β_5. In the $Eu_8Ga_{16-x}Ge_{30+x}$ samples, x defines the deviation from the 16:30 stoichiometry of Ga–Ge and varies from ~0.5 to 1. The β_1 sample with $x \sim 0.5$ (largest Ga content) shows the smallest charge carrier concentration and the largest power factor while the β_5 sample with $x \sim 1$ (smallest Ga content) shows the largest charge carrier concentration and the smallest power factor [38]. The electron transport properties of $Eu_8Ga_{16}Ge_{30}$-rc8105 are similar to the ones of β_4–β_5 $Eu_8Ga_{16-x}Ge_{30+x}$ and this indicates a similar electron concentration. $Ba_8Ga_{16}Ge_{30}$-rc41 displays a power factor smaller than that of $Ba_8Ga_{16}Ge_{30}$-Toberer [14].

Table 2 shows that the Seebeck coefficient of both $Ba_8Ga_{16}Ge_{30}$ are quite similar at 400 K while the resistivity of $Ba_8Ga_{16}Ge_{30}$-rc41 is approximately three times the value of the reference $Ba_8Ga_{16}Ge_{30}$-Toberer. This most likely arises from a lower density of $Ba_8Ga_{16}Ge_{30}$-rc41 obtained by SPS. The lower performances of the electron transport properties of $Eu_8Ga_{16}Ge_{30}$-rc8105 arises from its size (12 g), which is considerably larger than in previous work (3 g) and reflects scale-up difficulties caused by synthesis facilities dedicated to small size samples. Temperature gradients resulting from too small furnaces lead to inhomogeneities of composition/charge carriers concentration since $Eu_8Ga_{16}Ge_{30}$ exhibits a rather limited domain of thermal stability.

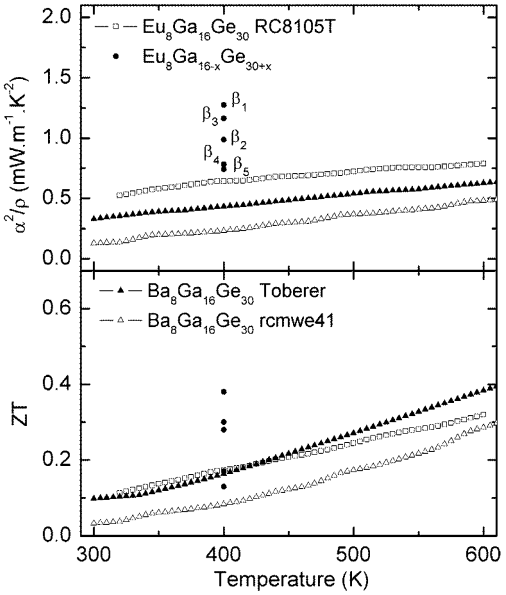

Figure 3 Thermal variations of the power factor (α^2/ρ) and figure of merit of $Eu_8Ga_{16}Ge_{30}$-rc8105 and $Ba_8Ga_{16}Ge_{30}$-rc41 compared to data extracted from literature measured on polycrystals. Data for polycrystalline $Ba_8Ga_{16}Ge_{30}$ "Toberer" are taken from Ref. [14], and $Eu_8Ga_{16-x}Ge_{30+x}$ from Ref. [38]

Table 2 Resistivity, Seebeck coefficient, thermal conductivity and lattice thermal conductivity of $Eu_8Ga_{16}Ge_{30}$-rc8105 and $Ba_8Ga_{16}Ge_{30}$-rc41 measured at 400 K and compared with results from literature (see text). The labeling of the samples β_i is taken from Ref. [38].

sample	ρ (mΩ cm)	α (μV K^{-1})	λ (W m^{-1} K^{-1})	λ_L (W m^{-1} K^{-1})
rc8105[a]	1.05	−82	1.5	0.7
β_5[a]	0.72	−75	2.4	1.3
β_4[a]	1.22	−95	1.4	0.8
β_2	1.28	−122	1.6	0.9
β_3	1.61	−126	1.4	0.9
β_1	2.06	−162	1.3	0.9
rc41[b]	3.13	−85	1.1	0.9
Toberer[b]	0.92	−63	1.4	0.3

[a] $Eu_8Ga_{16-x}Ge_{30+x}$ samples.
[b] $Ba_8Ga_{16}Ge_{30}$ samples.

The lattice thermal conductivity (λ_L) of $Eu_8Ga_{16}Ge_{30}$-rc8105 is very close to that of optimized β_1–β_3 $Eu_8Ga_{16-x}Ge_{30+x}$ while λ_L in $Ba_8Ga_{16}Ge_{30}$-rcmwe41 is in line with the value reported in Ref. [13]. On the other hand, λ_L of $Ba_8Ga_{16}Ge_{30}$-Toberer is surprisingly low. Table 2 shows that λ_L of these clathrates depends on the electron concentration, as already discussed in Ref. [38]. Briefly, this dependence is interpreted as arising from differences in the coupling between the vibration modes of Eu or Ba in their large cage and the heat-carrying acoustic phonons when the electron concentration changes. Finally, $Eu_8Ga_{16}Ge_{30}$-rc8105 has $ZT = 0.32$ at 600 K and $Ba_8Ga_{16}Ge_{30}$-rcmwe41 has $ZT = 0.29$ at 600 K and both compare well with literature [14, 38].

The temperature-dependent power factor and figure of merit of the samples $Mm_{0.7}Fe_{3.5}Ni_{0.5}Sb_{12}$-1696 and $Mm_{0.7}Fe_3CoSb_{12}$-1726 are compared to data from literature in Fig. 4. Unfortunately, λ of the latter sample could not be measured and thus no ZT values are displayed. The room temperature values of ρ, α, λ, and λ_L are reported in Table 3. The power factors of $Mm_{0.7}Fe_{3.5}Ni_{0.5}Sb_{12}$-1696 and $Mm_{0.7}Fe_3CoSb_{12}$-1726 are very similar. The slightly better value of $Mm_{0.7}Fe_3CoSb_{12}$-1726 does not arise from the replacement of Ni by Co but can simply be ascribed to a better sample quality: $Mm_{0.7}Fe_3CoSb_{12}$-1726 contains less secondary phases: ~10% (Mm_3Sb_4, Fe/$CoSb_2$) compared to ~15% (Mm_3Sb_4, Fe/$NiSb_2$) in $Mm_{0.7}Fe_{3.5}Ni_{0.5}Sb_{12}$-1696. These power factors are very close to the power factor of the reference materials $La_{0.7}Fe_3CoSb_{12}$ and $Ce_{0.7}Fe_3CoSb_{12}$ reported by Sales et al. in Ref. [7]. This is consistent with the composition of the mischmetall we used: 53 at% Ce, 21 at% La, 19 at% Nd, and 6 at%. Pr. The figure of merit of $Mm_{0.7}Fe_{3.5}Ni_{0.5}Sb_{12}$-1696 is with $ZT = 0.46$ is fairly close to that of $La_{0.7}Fe_3CoSb_{12}$. The difference to the data for $Mm_{0.8}Fe_3CoSb_{12}$ reported by Zhang et al. [28] can be explained as follows: the larger power factor of this latter reference sample is due to a much smaller electrical resistivity (see Table 3) and its larger ZT is in addition due to the unexpectedly low value of the lattice thermal conductivity, $\lambda_L = 0.8$ $Wm^{-1}K^{-1}$ at 300 K (Table 3).

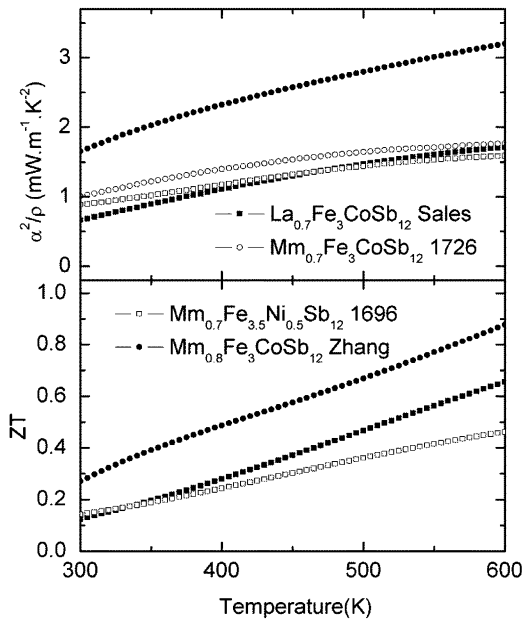

Figure 4 Thermal variations of the power factor (α^2/ρ) and figure of merit (ZT) of $Mm_{0.7}Fe_{3.5}Ni_{0.5}Sb_{12}$-1696 and $Mm_{0.7}Fe_3CoSb_{12}$-1726 compared to data extracted from literature (polycrystals). $La_{0.7}Fe_3CoSb_{12}$ values of Sales taken from Ref. [7] and $Mm_{0.8}Fe_3CoSb_{12}$ values of Zhang from Ref. [28].

5 Unicouple design Our above presented calculations have shown that an efficient TE generator requires high-quality contacts between the thermoelements and the metallic electrodes since otherwise part of the electric power is wasted by Joule heating. We followed an established procedure [5, 39] to tackle this problem. As diffusion barrier

Table 3 Resistivity, Seebeck coefficient, thermal conductivity, and lattice thermal conductivity of $Mm_{0.7}Fe_{3.5}Ni_{0.5}Sb_{12}$-1696 and $Mm_{0.7}Fe_3CoSb_{12}$-1726 measured at 300 K and compared with literature. $La_{0.7}Fe_3CoSb_{12}$, Sales data taken from Ref. [7] and $Mm_{0.8}Fe_3CoSb_{12}$, Zhang data taken from Ref. [28].

sample	ρ (mΩ cm)	α (μV K^{-1})	λ (W m^{-1} K^{-1})	λ_L (W m^{-1} K^{-1})
1696	0.93	90	1.9	1.2
1726	0.90	95	–	–
Sales	1.56	102	1.6	1.2
Zhang	0.64	105	1.8	0.8

Table 4 Comparison between measured and calculated open circuit voltage and specific output power for the couples $Eu_8Ga_{16}Ge_{30}$ rc8105 – $MmFe_{3.5}Ni_{0.5}Sb_{12}$-1696 and $Ba_8Ga_{16}Ge_{30}$ rcmwe41 – $Mm_{0.8}Fe_3CoSb_{12}$-1726. From top to bottom: unicouple number, area of the n-leg and p-leg, thermoelements length, cold temperature, hot temperature, contact resistivity, load resistance, measured U_{open}, calculated U_{open}, measured P_{es}, calculated P_{es}, calculated efficiency.

	rc8105–1696	rcmwe41–1726
No.	6	7
A_n (cm^2)	0.618	0.450
A_p (cm^2)	0.503	0.433
l (mm)	6	6
T_C (K)	323	323
T_H (K)	573	573
ρ_c (μΩ cm^2)	16	16
R_{load} (mΩ)	2.54	2.54
U_{open} (mV)	53.8	53.7
U_{open} (mV)	51.2	55.3
P_{es} (mW cm^{-2})	178	124
P_{es} (mW cm^{-2})	231	152
η (%)	2.9	1.7

and to ensure good wetability for brazing we first deposited a metallic intermediate layer on the end faces of the thermoelements. We chose electrochemical deposition because of its simplicity, efficiency and low cost. This restricted the choice of metallic layers to Ag, Cu, and Ni which can be easily deposited in aqueous solutions. Up to a temperature of approximately 590 K reached during brazing (see below), we did not detect any reaction between Ni and the skutterudites on the one side and between either Ni or Cu and the clathrates on the other side. We deposited a $\sim$10 μm Ni layer on the hot side because of better cycling properties. In a second step, we brazed each leg of the couple to a metallic electrode. To withstand the temperature of 573 K on the hot side during operation and to avoid overheating of the clathrate and the skutterudite during the brazing process in air, the Pb–Ag eutectic with a melting point of 577 K appeared as a good compromise. To withstand the 323 K at the cold side, the Sn–In eutectic which melts at 393 K was chosen: it is thermally and chemically stable at 323 K.

Another issue in the unicouple design is the stress induced by different coefficients of thermal expansion (CTE) of the thermoelements and the electrodes. Thus, we measured the CTE of $Mm_{0.7}Fe_{3.5}Ni_{0.5}Sb_{12}$ and $Eu_8Ga_{16}Ge_{30}$ by temperature-dependent powder X-ray diffraction between room temperature and 573 K and obtained CTE $= 11 \times 10^{-6}\,K^{-1}$ for both the skutterudite and the clathrate.

The fact that both CTE are the same means that the chosen materials can be easily paired in a unicouple and post facto supports our choice of materials. Brass has a larger CTE of $19 \times 10^{-6}\ K^{-1}$ but was nevertheless initially used as a hot side electrode and did not adversely affect the skutterrudite leg. However, the clathrate leg did not resist more than one or two thermal cycles up to 573 K and we therefore replaced the brass electrode by a nickel electrode which has a CTE of $13 \times 10^{-6}\,K^{-1}$ at 300 K. This solved the mechanical problems.

Figure 5 shows a sketch of the clathrate–skutterudite unicouple. A bottom brass block contains a heater cartridge (220 V, 175 W). A nickel electrode is screwed on the brass block. A type K thermocouple is placed in a 0.5 mm hole drilled in the Ni electrode. The clathrate and skutterudite legs are brazed to the nickel electrode on one side and to two thick copper electrodes on the other side. A thermocouple is inserted in a hole drilled into one of these copper electrodes to measure the cold side temperature. The two copper electrodes are thermally contacted to a copper platform by a heat conducting grease. The platform acts as a heat sink since it supports several passive convectors. To prevent short circuits between the copper electrodes, the copper platform is electrically insulated by a thin layer of Epotek H70E. Four threaded rods screwed in a metallic locking base support the copper platform. Glass wool is compressed between the locking base and the bottom brass block. It thermally insulates the unicouple from the locking base and it presses the unicouple against the copper platform to ensure a good thermal contact. The electrical current which is produced by the thermocouple is delivered to an electrical load connected

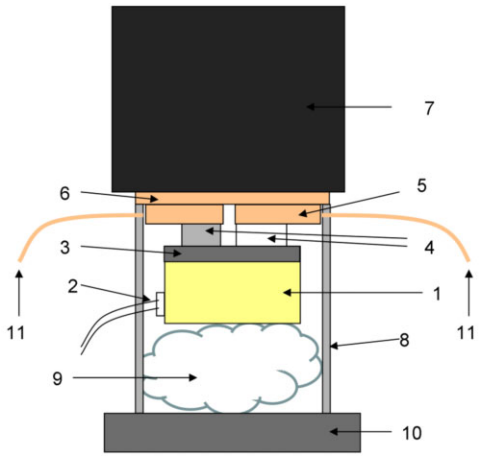

Figure 5 Schematic representation of the clathrate–skutterudite unicouple. Heat is flowing from bottom to top. (1) Brass block; (2) cartridge heater; (3) hot side nickel electrode; (4) clathrate and skutterudite thermoelements; (5) cold side copper electrode; (6) copper platform; (7) convector; (8) threaded rods; (9) glass wool; (10) locking base; (11) copper wires.

to the two upper copper electrodes. This load is constituted by two copper wires, 3 mm thick and 50 cm long, shortened on a calibrated 0.1 mΩ shunt. The total load resistance which is $R_{load} = 2.54$ mΩ mainly arises from the copper wires and nearly matches the internal resistance of the generator. A measurement of the voltage drop across the shunt by a microvoltmeter allows for a direct determination of the current and electrical power. Removal of the calibrated shunt and measurement of the voltage across the copper wires yields the open circuit voltage (U_{open}).

The internal resistance of the unicouple (R_{int}) was measured at room temperature by a four-probe technique, using the copper wires as current carrying electrodes (shunt removed) and the low-temperature side copper collectors as voltage sensing electrodes. The total contact resistance (R_c) at 300 K was determined by subtracting the resistance of each sample (R_{clath} and R_{skutt}) from the internal resistance: $R_c = R_{int} - (R_{clath} + R_{skutt})$ with R_{clath} and R_{skutt} derived from resistivity and accurate dimension measurements. The specific contact resistance is obtained from the relation $\rho_c = R_c((A_n + A_p)/8)$.

6 Unicouple operation and results Several unicouples were assembled with various samples, intermediate layers and brazings for the joins. During all these tests in air, the Pb–Ag brazing never showed any cracks. In the first tested unicouple without intermediate layer (N°1), we achieved $\rho_c = 520\ \mu\Omega\,cm^2$. By introducing a Ni/Cu intermediate layer deposited on the clathrate hot side ρ_c could be drastically lowered to $50\ \mu\Omega\,cm^2$ in unicouple N°2: this arises from the much better wetability by the brazing of the Ni/Cu layer. Tests 3–4 revealed the poor cyclability of the Ni/Cu layer. For unicouple No. 5, Ni intermediate layers

were deposited on both the hot and the cold side of both the skutterudite and the clathrate leg and this led to typical ρ_c values of 16 $\mu\Omega\,cm^2$. These are slightly lower than the 20–30 $\mu\Omega\,cm^2$ obtained by Zhao et al. [40] for joining $CoSb_3$ to a Mo–Cu electrode and the $\sim$20 $\mu\Omega\,cm^2$ reached by Caillat et al. [41] for joining $CeFe_4Sb_{12}$ or $CoSb_3$ to a Ti electrode. With these low contact resistivities, 97% of the available power can be retrieved by our device (see Fig. 2). Cycling the TE generator repeatedly up to 573 K leads to a decrease of the output power by $\sim$1% after each cycle. This decrease could be related to an overall increase of the contact resistance which could be due to a visually observed oxidation of the Pb–Ag brazing. Since no microscopic study of the hot side interface was carried out, we cannot exclude its deterioration to explain the decrease of power.

Figure 6 shows the specific output power (P_{es}) and the open circuit voltage (U_{open}) as function of the temperature difference (ΔT) for unicouple N°5 (best run). They vary approximately as $(\Delta T)^2$ and ΔT, respectively: such variations are expected for temperature independent transport coefficients. The maximum values $P_{es} = 178\,mW\,cm^{-2}$ and $U_{open} = 53.8\,mV$ are reached at the maximum temperature difference $\Delta T = 250\,K$ (value extrapolated from $\Delta T = 244\,K$). U_{open} obtained here is smaller than the 76.9 mV calculated with the transport data of $Eu_8Ga_{16}Ge_{30}$-ICT03 and $Yb_{0.4}Ce_{0.4}Fe_3CoSb_{12}$ taken from Refs. [19] and [35], respectively. This is a consequence of the smaller power factor of $Eu_8Ga_{16}Ge_{30}$-rc8105. The experimental specific output power is also smaller than the calculated one reported in Table 1 because both $Eu_8Ga_{16}Ge_{30}$-rc8105 and $Mm_{0.7}Fe_{3.5}Ni_{0.5}Sb_{12}$-1696 have a slightly smaller figure of merit than the two reference samples. Nevertheless, our results compare well with work on a Ba–Ga–Sn clathrate-based TE generator: $P_{es} = 178\,mW\,cm^{-2}$ with $\Delta T = 250\,K$ was obtained by Yamamoto et al. [42].

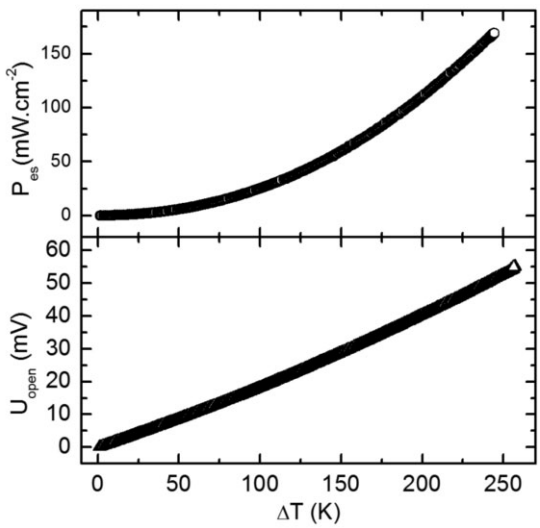

Figure 6 Specific power and open circuit voltage as a function of temperature for the $Eu_8Ga_{16}Ge_{30}$–$MmFe_{3.5}Ni_{0.5}Sb_{12}$ unicouple.

7 Comparison between model and experiments We also calculated the output power and open circuit voltage of the couples $Eu_8Ga_{16}Ge_{30}$-rc8105–$MmFe_{3.5}Ni_{0.5}Sb_{12}$-1696 and $Ba_8Ga_{16}Ge_{30}$-rcmwe41–$Mm_{0.8}Fe_3CoSb_{12}$-1726 from the experimentally determined transport properties (used for Figs. 3 and 4). To carry out these calculations, the area of each leg of the unicouple and the load resistance were taken equal to their experimental values and not optimized as in Table 1. Table 4 shows good agreement between the measured and calculated open circuit voltages. The agreement between the experimental and calculated specific output power is somewhat poorer: the experimental output power is systematically smaller by approximately 20% than the calculated one. This mainly arises from the fact that the model we use is one-dimensional and that it thus neglects the heat loss from the sides of the thermoelements by air convection and radiation. The actual temperature field is not uniform perpendicular to the main temperature gradient and the temperature of the sides is lower than at the thermoelements. Discrepancies between experiment and model ranging from 13% to 30% were also previously observed by El-Genk et al. [33]. Measurement uncertainties of the transport coefficients, the dimensions of the thermoelements, the contact resistivity and the resistive load will contribute to the observed discrepancy, too. The calculated efficiency is at most 2.9% and the actual efficiency ranges between 1% and 2%. It turns out that the n-leg over p-leg area ratio A_n/A_p of the $Eu_8Ga_{16}Ge_{30}$-rc8105–$MmFe_{3.5}Ni_{0.5}Sb_{12}$-1696 couple was accidentally close to the optimum and the calculated P_{es} would then only be 235 $mW\,cm^{-2}$.

8 Summary By using a simple one-dimensional model, we showed that a 5% efficiency and a specific electric power of nearly 450 $mW\,cm^{-2}$ could be obtained from a TE generator based on the best n-type clathrate and p-type skutterudite reported in literature if operated at a hot side temperature $T_H = 573\,K$. The clathrates $Eu_8Ga_{16}Ge_{30}$-rc8105 and $Ba_8Ga_{16}Ge_{30}$-rcmwe41 that were synthesized here reach $ZT = 0.32$ and $ZT = 0.29$, respectively, at 600 K. The skutterudites $Mm_{0.7}Fe_{3.5}Ni_{0.5}Sb_{12}$-1696 and $Mm_{0.7}Fe_3CoSb_{12}$-1726 display $ZT = 0.46$ and $ZT = 0.51$ at 600 K. The clathrate and skutterudite legs were brazed to a Ni electrode (compatible CTE) using Pb–Ag on the hot side and In–Sn on the cold side. Wetting and stability of the joins were improved by depositing a Ni layer on both legs. With these joins, contact resistivities of 16 $\mu\Omega\,cm^2$ were achieved. Our best run was obtained with the couple $Mm_{0.7}Fe_{3.5}Ni_{0.5}Sb_{12}$-1696 and $Eu_8Ga_{16}Ge_{30}$-rc8105 and yielded $P_{es} = 178\,mW\,cm^{-2}$ at $\Delta T = 250\,K$. Good agreement is obtained between the calculated and measured open circuit voltage ($\sim$50 mV), fair agreement for the specific output power ($\sim$200 $mW\,cm^{-2}$).

Acknowledgements Part of this work was funded by the European Network of Excellence "Complex Metallic Alloys" and the Austrian Science Fund (project TRP 176-N22). Support from the ESF networking program INTELBIOMAT and the Swiss

Federal Office of Energy is further acknowledged. The authors thank W. Schnelle for his help in setting up the unicouple during a temporary exhibition.

References

[1] K. Matsubara, Mater. Res. Soc. Symp. Proc. **691**, 327 (2002).
[2] J. Yang, in: Proc. 24th Int. Conf. on Thermoelectrics, Clemson, USA, 2005 (Institute of Electrical and Electronics Engineers), p. 155.
[3] J. Fairbanks, in: 6th European Conf. on Thermoelectrics (ECT2008), Paris, France, July 4–6, (2008), http://ect2008.icmpe.cnrs.fr/Contributions/0-PL-00-Fairbanks.pdf
[4] M. Saka and M. Asai, Patent JP 2002 266701A (Honda Motor Co., Japan, 2002).
[5] D. M. Rowe, CRC Handbook of Thermoelectrics (CRC Press, Boca Raton, 1995).
[6] T. Caillat, A. Borshchevsky, and J. P. Fleurial, in: Proc. 28th Intersociety Energy Conversion Engineering Conf. (IECEC '93), Atlanta, USA, 1993 (American Chemical Society), p. 1244.
[7] B. C. Sales, D. Mandrus, and R. K. Williams, Science **272**, 1325 (1996).
[8] G. S. Nolas, M. Kaeser, R. T. Littleton, and T. M. Tritt, Appl. Phys. Lett. **77**, 1855 (2000).
[9] G. S. Nolas, J. L. Cohn, G. A. Slack, and S. B. Schujman, Appl. Phys. Lett. **73**, 178 (1998).
[10] A. Saramat, G. Svensson, A. E. C. Palmqvist, C. Stiewe, E. Mueller, D. Platzek, S. G. K. Williams, D. M. Rowe, J. D. Bryan, and G. D. Stucky, J. Appl. Phys. **99**, 023708 (2006).
[11] M. Christensen, A. B. Abrahamsen, N. B. Christensen, F. Juranyi, N. H. Andersen, K. Lefmann, J. Andreasson, C. R. H. Bahl, and B. B. Iversen, Nature Mater. **7**, 811 (2008).
[12] H. Euchner, S. Pailhès, L. T. K. Nguyen, W. Assmus, F. Ritter, A. Haghighirad, Y. Grin, S. Paschen, and M. de Boissieu, Phys. Rev. B **86**, 224303 (2012).
[13] V. L. Kuznetsov, L. A. Kuznetsova, A. E. Kaliazin, and D. M. Rowe, J. Appl. Phys. **87**, 7871 (2000).
[14] E. S. Toberer, M. Christensen, B. B. Iversen, and G. J. Snyder, Phys. Rev. B **77**, 075203 (2008).
[15] X. Shi, J. Yang, S. Bai, J. Yang, H. Wang, M. Chi, J. R. Salvador, W. Zhang, L. Chen, and W. Wong-Ng, Adv. Funct. Mater. **20**, 755 (2010).
[16] X. Tang, P. Li, S. Deng, and Q. Zhang, J. Appl. Phys. **104**, 013706 (2008).
[17] H. Zhang, H. Borrmann, N. Oeschler, C. Candolfi, W. Schnelle, M. Schmidt, U. Burkhardt, M. Baitinger, J. T. Zhao, and Y. Grin, Inorg. Chem. **50**, 1250 (2011).
[18] M. Falmbigl, A. Grytsiv, P. Rogl, P. Heinrich, E. Royanian, and E. Bauer, J. Alloys Compd. **567**, 65 (2013).
[19] A. Bentien, S. Paschen, V. Pacheco, Y. N. Grin, and F. Steglich, in: Proc. 22nd International Conference on Thermoelectrics ICT2003, La Grand Motte, France, 2003 (IEEE), p. 131.
[20] S. K. Deng, X. F. Tang, and Q. J. Zhang, J. Appl. Phys. **102**, 043702 (2007).
[21] D. Cederkrantz, A. Saramat, G. J. Snyder, and A. E. C. Palmqvist, J. Appl. Phys. **106**, 074509 (2009).
[22] H. Anno, M. Hokazono, M. Kawamura, J. Nagao, and K. Matsubara, in: Proc. 21st Int. Conf. on Thermoelectrics, Long Beach, California, USA, 2002 (IEEE, Piscataway), p. 77.
[23] B. Chen, J. H. Xu, C. Uher, D. T. Morelli, G. P. Meisner, J. P. Fleurial, T. Caillat, and A. Borshchevsky, Phys. Rev. B **55**, 1476 (1997).
[24] G. P. Meisner, D. T. Morelli, S. Hu, J. Yang, and C. Uher, Phys. Rev. Lett. **80**, 3551 (1998).
[25] X. Shi, J. Yang, J. R. Salvador, M. Chi, J. Y. Cho, H. Wang, S. Bai, J. Yang, W. Zhang, and L. Chen, J. Am. Chem. Soc. **133**, 7837 (2011).
[26] G. Rogl, A. Grytsiv, P. Rogl, E. Bauer, M. B. Kerber, M. Zehetbauer, and S. Puchegger, Intermetallics **18**, 2435 (2010).
[27] B. Bourgoin, D. Bérardan, E. Alleno, C. Godart, E. Leroy, and O. Rouleau, J. Alloys Compd. **399**, 47 (2005).
[28] L. Zhang, A. Grytsiv, M. Kerber, P. Rogl, E. Bauer, and M. Zehetbauer, J. Alloys Compd. **490**, 19 (2010).
[29] K. Matsubara, in: Proc. 21st Int. Conf. Thermoelectrics, (ICT'02) (IEEE, 2002), p. 418.
[30] M. W. Gaultois, T. D. Sparks, C. K. H. Borg, R. Seshadri, W. D. Bonificio, and D. R. Clarke, Chem. Mater. **25**, 2911 (2013).
[31] V. Pacheco, R. Cardoso-Gil, L. Tepech-Carrillo, and Y. Grin, Corros. Sci. **53**, 2368 (2011).
[32] A. C. Sklad, M. W. Gaultois, and A. P. Grosvenor, J. Alloys Compd. **505**, L6 (2010).
[33] M. S. El-Genk and H. H. Saber, Energy Convers. Managem. **44**, 1069 (2003).
[34] C. A. Domenicali, J. Appl. Phys. **25**, 1310 (1954).
[35] D. Bérardan, E. Alleno, C. Godart, M. Puyet, B. Lenoir, H. Scherrer, R. Lackner, E. Bauer, L. Girard, and D. Ravot, J. Appl. Phys. **98**, 033710 (2005).
[36] V. Pacheco, A. Bentien, W. Carrillo-Cabrera, S. Paschen, F. Steglich, and Y. N. Grin, Phys. Rev. B **71**, 165205 (2005).
[37] D. Bérardan, E. Alleno, C. Godart, O. Rouleau, and J. Rodriguez-Carvajal, Mater. Res. Bull. **40**, 537 (2005).
[38] A. Bentien, V. Pacheco, S. Paschen, Y. N. Grin, and F. Steglich, Phys. Rev. B **71**, 165206 (2005).
[39] G. S. Nolas, J. Sharp, and H. J. Goldsmid, Thermoelectrics: Basic Principles and New Materials Developments (Springer, Berlin, Heidelberg, New York, 2001).
[40] D. G. Zhao, X. Y. Li, W. Jiang, and L. D. Chen, J. Inorg. Mater. **24**, 545 (2009).
[41] T. Caillat, A. Zoltan, L. Zoltan, and G. J. Snyder, in: PCT Int. Appl., WO 2002 089224 A1 20021107 (NASA, USA, 2002).
[42] A. Yamamoto, K. Kishimoto, K. Nagase, H. Obara, K. Ueno, T. Koyanagi, K. Akai, T. Taguchi, Y. Kouno, T. Fukuda, Y. Saiga, and T. Takabatake, unpublished (2010).

